

# Thermodynamic Routes to Ultralow Thermal Conductivity and High Thermoelectric Performance

Pai-Chun Wei, Chien-Neng Liao, Hsin-Jay Wu, Dongwang Yang, Jian He, Gill V. Biesold-McGee, Shuang Liang, Wan-Ting Yen, Xinfeng Tang, Jien-Wei Yeh, Zhiquan Lin,\* and Jr-Hau He\*

Thermoelectric (TE) research is not only a course of materials by discovery but also a seedbed of novel concepts and methodologies. Herein, the focus is on recent advances in three emerging paradigms: entropy engineering, phase-boundary mapping, and liquid-like TE materials in the context of thermodynamic routes. Specifically, entropy engineering is underpinned by the core effects of high-entropy alloys; the extended solubility limit, the tendency to form a high-symmetry crystal structure, severe lattice distortions, and sluggish diffusion processes afford large phase space for performance optimization, high electronic-band degeneracy, rich multiscale microstructures, and low lattice thermal conductivity toward higher-performance TE materials. Entropy engineering is successfully implemented in half-Huesler and IV–VI compounds. In Zintl phases and skutterudites, the efficacy of phase-boundary mapping is demonstrated through unraveling the profound relations among chemical compositions, mutual solubilities of constituent elements, phase instability, microstructures, and resulting TE properties at the operation temperatures. Attention is also given to liquid-like TE materials that exhibit lattice thermal conductivity at lower than the amorphous limit due to intensive mobile ion disorder and reduced vibrational entropy. To conclude, an outlook on the development of next-generation TE materials in line with these thermodynamic routes is given.

on various alternative energy technologies. Thermoelectric technologies are a particularly attractive option due to their direct heat to electricity energy conversion. Thermoelectric (TE) devices are made of degenerate semiconductors or semi-metals known as TE materials. A material's TE performance at temperature  $T$  is gauged by the dimensionless figure of merit,  $zT = \sigma S^2 T / (\kappa_L + \kappa_e)$ , where  $\sigma$ ,  $S$ ,  $\kappa_L$ , and  $\kappa_e$  are the electrical conductivity, Seebeck coefficient, and lattice and electronic thermal conductivities, respectively. Typically, TE devices made of materials with higher  $zT$  values possess better energy conversion efficiency. TE energy conversion efficiency can be calculated by the following:  $\eta_{TE} = \frac{(T_H - T_C)}{T_H} \frac{\sqrt{1 + \bar{zT}} - 1}{\sqrt{1 + \bar{zT}} + \frac{T_C}{T_H}}$ , where the

term  $\left(\frac{T_H - T_C}{T_H}\right)$  is the Carnot efficiency,  $\bar{zT}$  is the average device figure of merit, and  $T_H$  and  $T_C$  are the temperatures of the hot and cold ends, respectively.<sup>[1]</sup> Despite no known theoretical upper limit of  $zT$ ,

state-of-the-art TE materials exhibit a maximum  $zT$  below 3.0 due to the inherently counterindicated  $\{\sigma, S, \kappa_e\}$  and unsatisfactory  $\kappa_L$ . As a result, the energy conversion efficiency of


## 1. Introduction

The increasing global energy demand along with environmental concerns of using fossil fuels has spurred vigorous research

Dr. P.-C. Wei, Prof. J.-H. He  
Computer, Electrical, and Mathematical Sciences  
and Engineering Division  
King Abdullah University of Science and Technology (KAUST)  
Thuwal 23955-6900, Saudi Arabia  
E-mail: jrhaue@cityu.edu.hk

Prof. C.-N. Liao, Prof. J.-W. Yeh  
High Entropy Materials Center  
Department of Materials Science and Engineering  
National Tsing Hua University  
Hsinchu, 30013 Taiwan, ROC

Prof. H.-J. Wu, W.-T. Yen  
Department of Materials Science and Engineering  
National Chiao Tung University  
Hsinchu, 30010 Taiwan, ROC

 The ORCID identification number(s) for the author(s) of this article can be found under <https://doi.org/10.1002/adma.201906457>.

Dr. D. Yang, Prof. X. Tang  
State Key Laboratory of Advanced Technology for  
Materials Synthesis and Processing  
Wuhan University of Technology  
Wuhan 430070, China

Prof. J. He  
Department of Physics and Astronomy  
Clemson University  
Clemson, SC 29634-0978, USA

G. V. Biesold-McGee, S. Liang, Prof. Z. Lin  
School of Materials Science and Engineering  
Georgia Institute of Technology  
Atlanta, GA 30332, USA  
E-mail: zhiquan.lin@mse.gatech.edu

Prof. J.-H. He  
Department of Materials Science and Engineering  
City University of Hong Kong  
Kowloon, Hong Kong

DOI: 10.1002/adma.201906457

state-of-the-art TE devices is far below the Carnot efficiency and unable to rival those of other sustainable energy conversion technologies, thereby impeding broader use of TE technology.

The core of TE materials research is decoupling the counter-indicated  $\{\sigma, S, \kappa_e\}$ , which can be understood and undertaken in the context of Boltzmann transport theory and the Wiedemann–Franz relation.<sup>[2–5]</sup> Specifically,  $S$  is enhanced in optimizing electronic band structure, classical and quantum size effects, electron energy band filtering, resonant levels, and energy-dependent impurity scattering to name a few.  $\sigma$  is governed by the carrier concentration ( $n$ ) and carrier mobility ( $\mu$ ). To alleviate the trade-off between  $\sigma$  and  $S$ , carrier pocket engineering, band convergence, modulation doping, and interfacial effects have been implemented with success.<sup>[6]</sup> To date, it remains a delicate task to balance the material requests for optimal  $n$ ,  $S$ ,  $\kappa_e$ , bandgap, band effective mass, and bipolar effect.<sup>[4]</sup> Notably,  $\kappa_L$  is relatively independent of  $\{\sigma, S, \text{ and } \kappa_e\}$  because  $\kappa_L$  is carried by phonons (aka, the normal modes of lattice vibrations). The most effective strategies to reduce  $\kappa_L$ <sup>[7–11]</sup> have proven to be the inclusion of hierarchical microstructures such as atomic-scale point defects, nanoscale precipitates, and mesoscale grain boundaries.<sup>[12]</sup> Reduced  $\kappa_L$  is not only conducive to attaining higher  $zT$  values but is also helpful in retaining a larger temperature gradient across the TE material, leading to a higher Carnot efficiency.<sup>[13]</sup>

Tremendous efforts have been exerted to develop high- $zT$  TE materials. In an effort to minimize overlap with the many existing review articles in the field,<sup>[4,6,14–29]</sup> this topical review is written from a different perspective: thermodynamic routes. This perspective focuses on how fundamental thermodynamics and phase diagrams can help achieve better TE materials. We survey and examine the recent advances in line with the emerging paradigms: i) entropy engineering, ii) phase-boundary mapping, and iii) liquid-like thermoelectrics. Accordingly, the main body of this article consists of three sections.

Before examining the recent advances of these paradigms in detail, we present some general thoughts in the context of thermodynamics. First, entropy engineering is a synergy of high-entropy alloys (HEAs) and conventional TE materials research. HEAs refer to crystalline solid solutions containing at least five principal elements with the atomic percentage of each element between 5% and 35%.<sup>[30–32]</sup> From a composition perspective, HEAs are at or near the center of the high multinary phase diagram. From the material functionality perspective, it is plausible to “define” HEA as a material that exhibits these four core effects: high configurational entropy, sluggish atomic diffusion, severe lattice distortions, and the cocktail effect. These core effects of HEA are well aligned with the material requirements for good thermoelectrics.<sup>[33–40]</sup> Specifically, high configurational entropy elicits: i) extended solubility limits of specific elements and high-symmetry crystal structure, thereby expanding the phase space for performance optimization and favoring good electronic band structure; ii) severely distorted crystal lattice, thereby softening and impeding heat-carrying phonons; and iii) slow diffusion processes, thereby creating rich multiscale microstructures prerequisite for reducing the lattice thermal conductivity. One downside of these core effects is the degradation of charge carrier mobility, which must be compensated by other physical properties in practice (Table 1).



**Pai-Chun Wei** is a research scientist affiliated to King Abdullah University of Science and Technology (KAUST). He received B.S. (2002), M.S. (2004), and Ph.D (2009) degrees from the Department of Materials Science and Engineering at National Tsing Hua University (Taiwan) and started his academic carrier at the

institute of physics, Academia Sinica (Taiwan) in 2011. His research interests include molecular beam epitaxy of III–V semiconductors, single-crystal growth, lattice dynamics of low-thermal-conductivity materials, and thermoelectric materials.



**Zhiquan Lin** is a Professor in the School of Materials Science and Engineering at the Georgia Institute of Technology. He received his Ph.D. in polymer science and engineering from the University of Massachusetts, Amherst in 2002. His research interests include solar cells, photocatalysis, electrocatalysis, batteries,

semiconductor organic–inorganic nanocomposites, conjugated polymers, block copolymers, hierarchical structure formation and assembly, surface and interfacial properties, multifunctional nanocrystals, and Janus nanostructures.



**Jr-Hau He** is a Professor in the Department of Materials Science and Engineering at City University of Hong Kong. He received his B.S. and Ph.D. degrees from National Tsing Hua University in 1999 and 2005, respectively. He has been a pioneer in energy materials and memristors for neuromorphic computing. He has conducted highly inter-

disciplinary research to bridge the gaps between various research fields and between academia and industry.

The general significance of phase-boundary mapping lies in the fact that alloying and doping remain the mainstream protocol to optimize TE properties. The scope of alloying and doping and the tolerance of off-stoichiometry (aka, self-doping) are restricted by the solubility limit and, in turn, governed by

**Table 1.** A brief summary of the advantages and disadvantages of three emerging paradigms of TE materials research: entropy engineering, phase-boundary mapping, and liquid-like thermoelectrics.

Emerging paradigms of TE materials	Advantages	Disadvantages
Entropy engineering	<ul style="list-style-type: none"> <li>i) Extended phase space for materials performance optimization</li> <li>ii) Severe crystal lattice distortion leading to low lattice thermal conductivity</li> <li>iii) Sluggish diffusion processes facilitating the formation of rich multiscale microstructures</li> </ul>	<ul style="list-style-type: none"> <li>i) Reduced carrier mobility must be compensated by improvement of other electrical transport properties</li> </ul>
Phase-boundary mapping	<ul style="list-style-type: none"> <li>i) Guided joint effort of extrinsic and self-doping for materials performance optimization</li> <li>ii) Solubility limit and secondary phase(s) under control</li> </ul>	<ul style="list-style-type: none"> <li>Fine mapping of phase diagram, especially at low temperatures, is time consuming and error-prone</li> </ul>
Liquid-like thermoelectrics	<ul style="list-style-type: none"> <li>i) Damped transverse phonon modes</li> <li>ii) Strong static or dynamic scattering of phonons</li> </ul>	<ul style="list-style-type: none"> <li>Structural instability under high thermal and/or electric field</li> </ul>

thermodynamics. Once the composition crosses the boundary of single-phase region in phase diagram, nonstoichiometric defects and secondary phase shall form. Phase-boundary mapping has been implemented to guide the control of extrinsic doping and off-stoichiometry,<sup>[41–46]</sup> in which we were able to determine the highest tolerance of off-stoichiometry for Zintl phases, the maximum filling fraction limits (FFLs) of specific guest elements in skutterudites, and how the variations of nominal composition and the formation of secondary phase affect the TE properties.

Unlike most state-of-the-art TE materials that are electron-based semiconductors or semimetals, liquid-like TE materials are mixed electronic ionic conductors. In a mixed electronic ionic conductor, the liquid-like (premelted) sublattice interpenetrates the remaining crystalline sublattice, while ionic migration coexists with high TE performance. Hence, liquid-like TE materials are hybrid in both electrical conduction (electrons + ions) and crystal structure (liquid-like sublattice + crystalline sublattice), giving rise to interesting thermodynamics and transport properties. As known,  $\kappa_L$  approaches the amorphous limit when the phonon mean free path (MFP) is reduced to the interatomic spacing by various phonon scattering mechanism. Can  $\kappa_L$  be reduced below the amorphous limit? The TE study of liquid-like TE materials points toward a new solution. In a solid, heat is generally carried by longitudinal and transverse waves, whereas transverse waves are not sustained in a liquid. Liquid-like TE materials are found to have measured isobaric heat capacity  $C_p$  much lower than the classic Dulong–Petit limit at high temperatures.<sup>[47–52]</sup> It is argued that at high temperatures the mobile ions are delocalized, and the loss of transverse (shear) modes lowers the  $C_p$ ; in addition, the cationic disorder strongly scatters the phonons, yielding ultralow  $\kappa_L$ . Note that on the liquid-like sublattice, the mobile ions are greatly

outnumbered by the available (vacant) sites, implying native configurational entropy. The reduced heat capacity reflects the reduction of vibrational entropy.

## 2. High-Entropy Thermoelectric Materials

Entropy engineering is a recently proposed alloying approach to developing high-performance TE materials. Considering a multicomponent crystalline solid solution, the configurational entropy (entropy of mixing) is given by  $\Delta S_{\text{conf}} = -R \sum_{i=1}^n X_i \ln X_i$ ,<sup>[53]</sup> in which  $n$  is the number of components,  $X_i$  is the molar fraction of the  $i$ th component, and  $R$  is the gas constant. The contribution of entropy of mixing,  $-T\Delta S_{\text{conf}}$ , offsets the strain energy and thus stabilizes single-phased crystalline solid solution. In general, HEAs tend to form solid solutions with high-symmetry crystal structure (body-centered cubic or face-centered cubic), which is thermoelectrically favored in terms of promoting electron band degeneracy. To form a single-phased solid solution, the alloying elements must have similar electronic and chemical properties as well as small difference in atomic size in accordance with the classic Hume–Rothery rules, though some material requirements can be somewhat compromised due to high-entropy effects. A solubility parameter  $\delta$  that depends on the material's shear modulus, lattice constants, and mismatch of atomic radii has been proposed to account for the internal strain energy and atomic solubility of multicomponent materials.<sup>[54]</sup> Regarding TE materials, pseudobinary systems with low  $\delta$  values (e.g., (Cd/Hg)Te, Pb(S/Se), (Rh/Ir)Sb<sub>3</sub>, Cu<sub>2</sub>(S/Se), Cu<sub>2</sub>(Se/Te), (Bi/Sb)<sub>2</sub>Te<sub>3</sub>, (Cu/Ag)InTe<sub>2</sub>, and (Cu/Ag)GaTe<sub>2</sub>) tend to form complete solid solutions, while those with very large  $\delta$  values (e.g., Pb(S/Te)) have limited atomic solubility and are inclined to have phase separation. In other words, materials with higher  $\delta$  values require a larger number of alloying elements, i.e., a higher  $T\Delta S_{\text{conf}}$ , to obtain single-phased high-symmetry solid solutions.<sup>[54]</sup>

The interplay of random atomic mixing and high-symmetry crystal structure profoundly affects the TE properties. For instance, doping multiple elements into a high-symmetry lattice tends to facilitate multiple electronic bands near the Fermi level (aka, band degeneracy or band convergence), thereby enhancing the  $S$  at optimal carrier concentration. Meanwhile, highly disordered atomic arrangement causes severe lattice distortions and strain-field fluctuations that lead to suppressed  $\kappa_L$ . The suppression of  $\kappa_L$  by increasing configurational entropy in various TE material systems is demonstrated in **Figure 1a**. Interestingly, the reduction of  $\kappa_L$  is more significant for the those with high initial thermal conductivities, such as half-Heusler ZrNiSn-based materials. In contrast, increased configurational entropy has much less effect on the  $\kappa_L$  of liquid-like TE materials, which have very low intrinsic thermal conductivity. This is not a surprise because liquid-like TE materials have very low site occupancy on the liquid-like (mobile ion) sublattice, possessing fairly high native configurational entropy even without doping or alloying. In **Figure 1b**, the structural symmetries of Cu<sub>2</sub>S<sub>0.5</sub>Te<sub>0.5</sub>, Cu<sub>2</sub>S<sub>0.5</sub>Se<sub>0.5</sub>, and Cu<sub>2</sub>S<sub>1/3</sub>Se<sub>1/3</sub>Te<sub>1/3</sub> increase from monoclinic to hexagonal due to increasing configurational entropy. With increasing crystal lattice symmetry,  $S$  values rise significantly. Again, the  $S$  enhancement by increasing

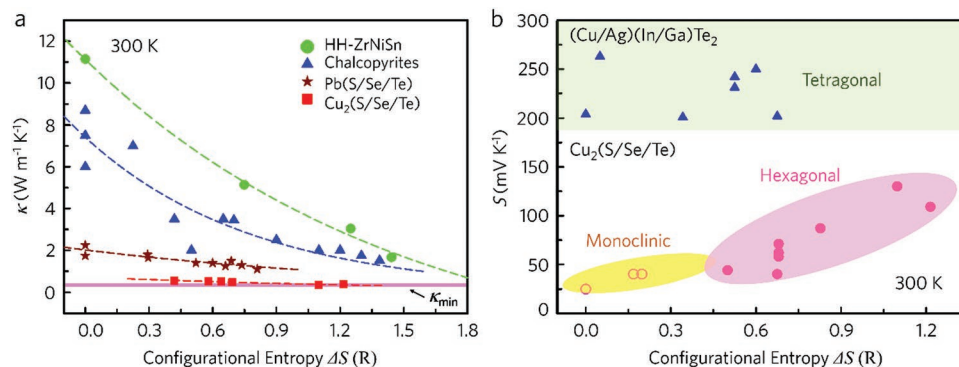


**Figure 1.** The reduced lattice thermal conductivity ( $\kappa_L$ ) and improved Seebeck coefficient ( $S$ ) in multicomponent TE materials at room temperature. a)  $\kappa_L$  as a function of the configurational entropy. The  $\kappa_{\min}$  is the amorphous limit of thermal conductivity and the dashed lines are guides for the eyes. b)  $S$  as a function of the configurational entropy in  $(\text{Cu/Ag})(\text{In/Ga})\text{Te}_2$  and  $\text{Cu}_2(\text{S/Se/Te})$ -based materials. Adapted with permission.<sup>[54]</sup> Copyright 2017, Wiley-VCH.

configurational entropy is less significant for  $(\text{Cu/Ag})(\text{In/Ga})\text{Te}_2$ , which have high initial crystal symmetry and intrinsic cationic site disorder.

A systematic entropy engineering study was conducted in  $(\text{Sn,Ge,Pb,Mn})\text{Te}$  alloys.<sup>[55]</sup> The room-temperature  $\Delta S_{\text{conf}}$ ,  $S$ , carrier concentration ( $n_H$ ), carrier mobility ( $\mu_H$ ), and  $\kappa_L$  of these  $(\text{Sn,Ge,Pb,Mn})\text{Te}$  alloys are plotted versus the number of alloy elements ( $N = 2-5$ ) in **Figure 2**. It is known that increasing the number of alloying elements is beneficial for increasing the  $|S|$  and  $n_H$  of  $\text{Pb}(\text{Te/Se})$ -based materials, due to band convergence and the appearance of additional energy band,<sup>[35,56-58]</sup> meanwhile, the increasing mass and strain fluctuations degrade  $\mu_H$  and suppress  $\kappa_L$ . The dominant scattering mechanism

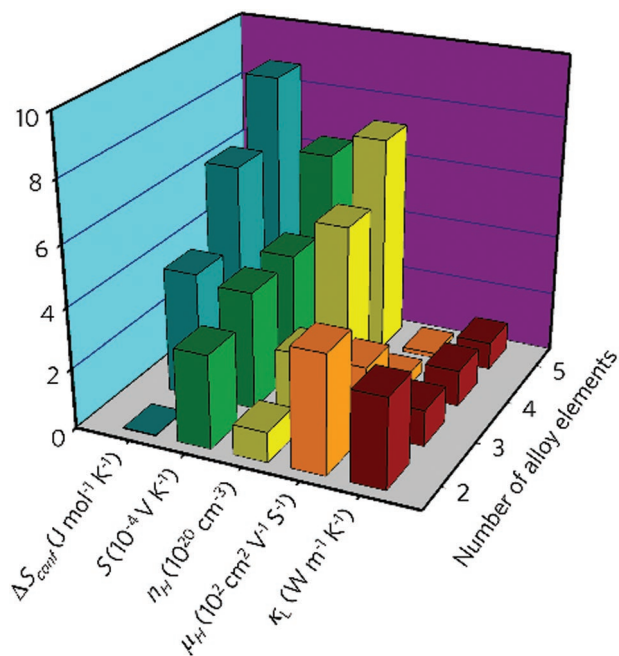


**Figure 2.** The entropy of mixing ( $\Delta S_{\text{conf}}$ ), Seebeck coefficient ( $S$ ), carrier concentration ( $n_H$ ), carrier mobility ( $\mu_H$ ), and lattice thermal conductivity ( $\kappa_L$ ) at room temperature for  $\text{SnTe}$ ,  $\text{Sn}_{0.8}\text{Ge}_{0.2}\text{Te}$ ,  $\text{Sn}_{0.7}\text{Ge}_{0.2}\text{Pb}_{0.1}\text{Te}$ , and  $(\text{Sn}_{0.7}\text{Ge}_{0.2}\text{Pb}_{0.1})_{0.9}\text{Mn}_{0.1}\text{Te}$ . Data set from ref. [55]. Adapted with permission.<sup>[55]</sup> Copyright 2018, Wiley-VCH.

smoothly crossed over from electron-phonon coupling to alloying scattering with the increasing number of alloying elements.<sup>[58]</sup> The solubility of Mn was substantially extended due to high configurational entropy effect. The TE properties of high-entropy  $(\text{Sn,Ge,Pb,Mn})\text{Te}$  alloys were improved by varying the Mn and Sn contents.<sup>[58]</sup> Through decreasing Sn vacancies, the PF at high temperatures was significantly increased due to the enhanced  $S$ , leading to a peak  $zT$  value of 1.42 at 900 K when  $\gamma = 0.03$ .<sup>[58]</sup> The caveat is that the configurational entropy should be high enough to take advantage of the core effect of HEA yet low enough, so the degraded carrier mobility can be compensated by higher carrier concentration and band convergence.

While a single-phased solid solution is generally preferred in TE materials' research, the presence of secondary phase is neither at odds with the spirit of HEA nor necessarily detrimental to the TE performance. As is often the case, the presence of secondary phase in situ formed in a high-entropy host matrix is thermoelectrically favored; in that a wide spectrum of heat-carrying phonons is effectively scattered by defects with diverse characteristic length scales. In the example discussed above,<sup>[58]</sup> increasing the Mn content would risk the formation of secondary phases such as  $\text{GeTe}$ ,  $\text{MnTe}$ , and  $\text{Ge}$  in the  $(\text{Sn,Ge,Pb,Mn})\text{Te}$  alloys. Although the  $\mu_H$  was unavoidably impacted by the secondary phases, the  $S$  was enhanced and  $\kappa_L$  was reduced below the amorphous limit, raising the peak  $zT$  value from 1.07 to 1.27 at 900 K when  $x = 0.25$ . For the  $(\text{Pb,Sn,Ge})\text{Te}$  multinary compounds,  $\text{Pb}_{0.25}\text{Sn}_{0.25}\text{Ge}_{0.5}\text{Te}$  lies in the miscibility gap of  $\text{Ge-PbTe-SnTe}$  pseudoternary phase diagram;  $\text{Pb}_{0.25}\text{Sn}_{0.25}\text{Ge}_{0.5}\text{Te}$  is decomposed into Pb-rich ( $\text{Pb}_{0.33}\text{Sn}_{0.3}\text{Ge}_{0.37}\text{Te}$ ) and Ge-rich ( $\text{Pb}_{0.1}\text{Sn}_{0.17}\text{Ge}_{0.73}\text{Te}$ ) phases when treated at 673 K;<sup>[36]</sup> the heterogeneous phase boundaries elicit strong phonon scattering and thus significantly reduced  $\kappa_L$ .

Most HEAs exhibit satisfactory phase stability at high temperatures, thereby ensuring the thermal and chemical stability of secondary phase(s) in situ formed. Further systematic study of the phase instability and the resulting impact on the transport properties of high-entropy TE materials shall pave the way for high-entropy TE composites. The success of such a "high-entropy TE composites" approach is hinged upon the detailed



knowledge of high-temperature high-multinary phase diagram. In this regard, phase-boundary mapping is an effective tool of phase design and also is the theme of the following section.

### 3. Thermoelectric Phase-Boundary Mapping

For decades, it has been known that degenerate semiconductors and semimetals possess good thermoelectric properties for a variety of reasons.<sup>[59]</sup> First, the presence of a bandgap ensures the magnitude of Seebeck coefficient, native defects (e.g., vacancies, antisites, interstitials, grain boundaries, to name a few) and extrinsic dopants that optimize the Fermi level and the carrier concentration.<sup>[4,60,61]</sup> Additionally, defects scatter heat-carrying phonons to lower the lattice thermal conductivity. Note that the formation energies of native and extrinsic defects are temperature dependent, affording a new control parameter for performance optimization. In addition, the high configurational entropy effect tends to extend the solubility limit of specific elements.<sup>[62,63]</sup> When the nominal composition crosses the phase boundary, a secondary phase is formed. Various studies have demonstrated that the formation of micro- or nanoscale precipitates along grain boundaries can greatly enhance phonon scattering, especially at low temperatures.<sup>[16,64–66]</sup> The grain boundaries decrease the  $\mu_H$ , but the degradation is minimal in the case of semicoherent or coherent grain boundaries.<sup>[67,68]</sup>

The scope of off-stoichiometry, doping, and alloying is restricted by the phase stability- and temperature-limited solubility. Detailed knowledge of high multinary (composition and temperature) phase diagrams is essential for TE materials' research. Though many conventional TE synthesis techniques (such as hot pressing and spark plasma sintering) cannot be represented by phase diagram due to their nonequilibrium nature,<sup>[69–72]</sup> phase diagrams are still an important guide for their design. In practice, phase-boundary mapping helps establish the relationships between solubility limits, non-stoichiometric defects, secondary precipitates and TE properties (Table 1). Once the solubilities and phase boundaries are known, the solubility limit of the dopant, precipitation temperature, and synthesis procedure can be optimized for peak TE performance.  $\text{Bi}_2\text{Te}_3$ ,<sup>[73,74]</sup>  $\text{PbTe}$ ,<sup>[75,76]</sup>  $\text{Zn}_4\text{Sb}_3$ ,<sup>[77,78]</sup> and  $\text{GeTe}$ <sup>[79,80]</sup>

are conventional high- $zT$  binary compounds in which the constituent atoms have certain mutual solubility. Heavy doping and large off-stoichiometry are routinely used to optimize the TE properties. In contrast, line compounds such as Zintl phases and skutterudites have practically low mutual solubility between the constituent elements, low tolerance of off-stoichiometry, and a highly complex phase diagram, all of which make the approach to TE property optimization different.<sup>[41,42,81,82]</sup>

Phase-boundary mapping is an effective tool to guide the experimental efforts of doping and off-stoichiometry in line compounds. For example,  $\text{Ca}_9\text{Zn}_{4+x}\text{Sb}_9$  demonstrates good TE performance in the mid-temperature range.<sup>[41]</sup> It has the highest  $zT$  when the nominal composition ( $\text{Ca}_9\text{Zn}_{4.6}\text{Sb}_9$ ,  $zT = 1.1$  at 875 K) falls in the two-phase  $\text{CaZn}_2\text{Sb}_2 + \text{Ca}_9\text{Zn}_{4.5-5}\text{Sb}_9$  region of the Ca–Zn–Sb ternary phase diagram. The  $\text{CaZn}_2\text{Sb}_2$  precipitate in 9–4–9 phase is important because the resulting heterointerfaces cause strong phonon scattering that dramatically reduces  $\kappa_L$ . The presence of  $\text{CaZn}_2\text{Sb}_2$  also leads to a decreased carrier concentration that simultaneously optimizes  $\sigma$  and  $S$ . The lowest  $\kappa_L$  achieves  $\approx 0.4 \text{ W m}^{-1} \text{ K}^{-1}$  when  $T > 800 \text{ K}$ , which is even lower than the amorphous limit.<sup>[83]</sup> It is argued that the ultralow  $\kappa_L$  originates from anomalously low Lorentz factors or strong electron–phonon interactions,<sup>[84]</sup> which merits further investigation.

Phase-boundary mapping has also been applied to manipulate the  $zT$  of Zintl phase  $\text{Mg}_3\text{Sb}_2$ .<sup>[42,43]</sup> Although  $\text{Mg}_3\text{Sb}_2$  appears to be a line compound,<sup>[85]</sup> there is still some mutual solubility between Mg and Sb. As shown in Figure 3a, the mutual solubility increases with increasing temperature, especially above 700 K. In fact, the inclusion of excess Mg or Sb in  $\text{Mg}_3\text{Sb}_2$  can dramatically change the electrical properties of  $\text{Mg}_3\text{Sb}_2$ . For example, a p-type to n-type transition occurs when there is excess Mg (Figure 3a). n-Type  $\text{Mg}_{3+x}\text{Sb}_2$  is known to have better TE performance and attributed to the presence of Mg interstitials.<sup>[43]</sup> Recent defect formation energy calculations along with phase-boundary mapping corroborate that the Mg interstitials are not sufficient to compensate positive charge carriers and yield n-type conductance.<sup>[42]</sup> Rather, the excess free electron carriers come from the suppression of Mg vacancies by excess Mg. These results are crucial for developing  $\text{Mg}_3\text{Sb}_2$ -based higher-performance TE materials. For Bi or Te-doped

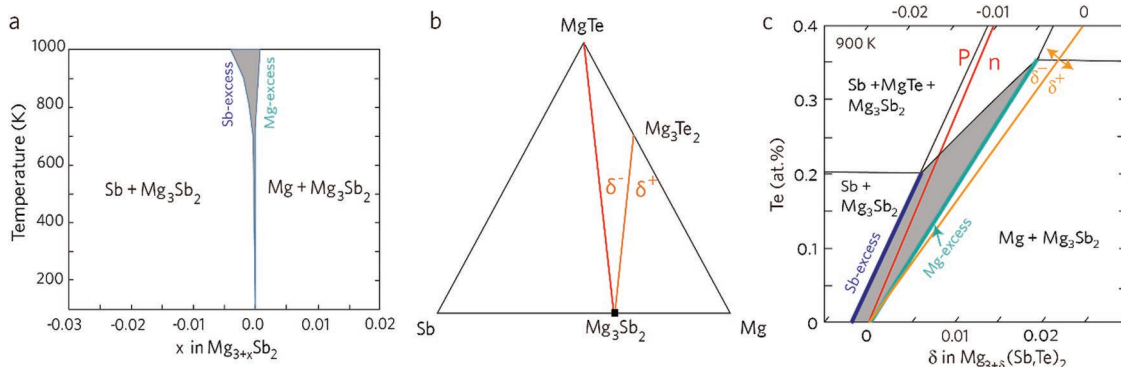


**Figure 3.** a) The binary Mg–Sb phase diagram, showing the Sb-excess and Mg-excess  $\text{Mg}_3\text{Sb}_2$ . b) The ternary Mg–Sb–Te phase diagram overlay with the position of  $\text{Mg}_{3+x}(\text{Sb},\text{Te})_2$ . c) The magnified phase diagram near the  $\text{Mg}_3\text{Sb}_2$  single-phase region (denoted by the filled gray color). The purple line indicates the Mg-excess boundary while the blue line shows the Sb-excess boundary. A red line further highlights the p–n transition border. Adapted with permission.<sup>[42]</sup> Copyright 2018, Elsevier.

$\text{Mg}_3\text{Sb}_2$ , p-type  $\text{Mg}_3\text{Sb}_2$  only attains a  $zT$  of  $<0.4$  (800 K), while the  $zT$  value of n-type  $\text{Mg}_3\text{Sb}_2$  is as high as 1.4.<sup>[42]</sup>

The n-type behavior of  $\text{Mg}_3\text{Sb}_2$  is rooted in the phase diagram. Figure 3b shows the isothermal section of the Mg–Sb–Te ternary system, in which the p–n transition boundary is highlighted by a red line while the stoichiometric composition ( $\delta = 0$ ) of  $\text{Mg}_{3+x}\text{Sb}_{2-y}\text{Te}_y$  is denoted by the orange line. The single-phase region of  $\text{Mg}_{3+x}\text{Sb}_{2-y}\text{Te}_y$  is further emphasized in Figure 3c, in which the blue line and green line delineate the Sb and Mg solubility limits of  $\text{Mg}_{3+x}\text{Sb}_{2-y}\text{Te}_y$ , respectively. Clearly,  $\text{Mg}_{3+x}\text{Sb}_{2-y}\text{Te}_y$  with excess Sb and  $\delta < 0$  will always be p-type while having excess Mg will make it n-type. Notice that when  $\text{Mg}_{3+x}\text{Sb}_{2-y}\text{Te}_y$  is in the  $\text{Mg}_3\text{Sb}_2$  single-phase region, the sample could be n-type but have  $\delta < 0$ .

A similar p–n transition in Cu– $\text{Bi}_2\text{Te}_3$  has been revealed by phase-boundary mapping.<sup>[86]</sup> As shown in Figure 4a, the  $\text{Bi}_2\text{Te}_3$  single-phase region has a clear nonsymmetrical equilibrium solubility of Cu in  $\text{Bi}_2\text{Te}_3$ . In the single-phase region, Cu-doped  $\text{Bi}_2\text{Te}_3$  samples (e.g.,  $(\text{Bi}_2\text{Te}_3)_{0.99}(\text{Cu}_2\text{Te})_{0.01}$ ) usually have positive  $S$  at 300 K due to the excess hole carriers (Figure 4b). When the amount of Cu exceeds the solubility limit, Cu–Te-based

secondary precipitates will appear in the  $\text{Bi}_2\text{Te}_3$  matrix. As shown in Figure 4b,c, the appearance of Cu–Te-based secondary precipitates changes the sign of  $S$ , indicating that they compensate the excess holes and lead to the n-type behavior. The appearance of secondary precipitates also has a pronounced effect on reducing  $\kappa_1$ . For example, the  $(\text{Bi}_2\text{Te}_3)_{0.9}(\text{Cu}_2\text{Te})_{0.1}$  sample exhibits a lamellar structure composed of  $\text{Bi}_2\text{Te}_3$  and  $\text{Cu}_7\text{Te}_5$  (Figure 4c). The lamellar micromorphology will additionally induce interfacial phonon scattering that is effective at reducing  $\kappa$ . Interestingly, the n-type  $(\text{Bi}_2\text{Te}_3)_{1-x}(\text{Cu}_2\text{Te})_x$  sample with  $x = 0.09$  has an almost temperature invariant  $zT \approx 1.0$  (Figure 4b), which is ideal for high-efficiency TE device fabrication.

$\text{CoSb}_3$ -based filled skutterudites are considered the most promising mid-temperature TE materials fulfilling the “phonon–glass–electron–crystal” concept and have been used in the automotive industry for waste heat recovery. For filled skutterudites, the most common strategy to maximize  $zT$  is to achieve the FFL.<sup>[81,82]</sup> However, the FFL is typically low and thermodynamically constrained. Hence, phase-boundary mapping is adopted. As shown in Figure 5a,b, the relationship between the FFL of skutterudites and secondary phases in

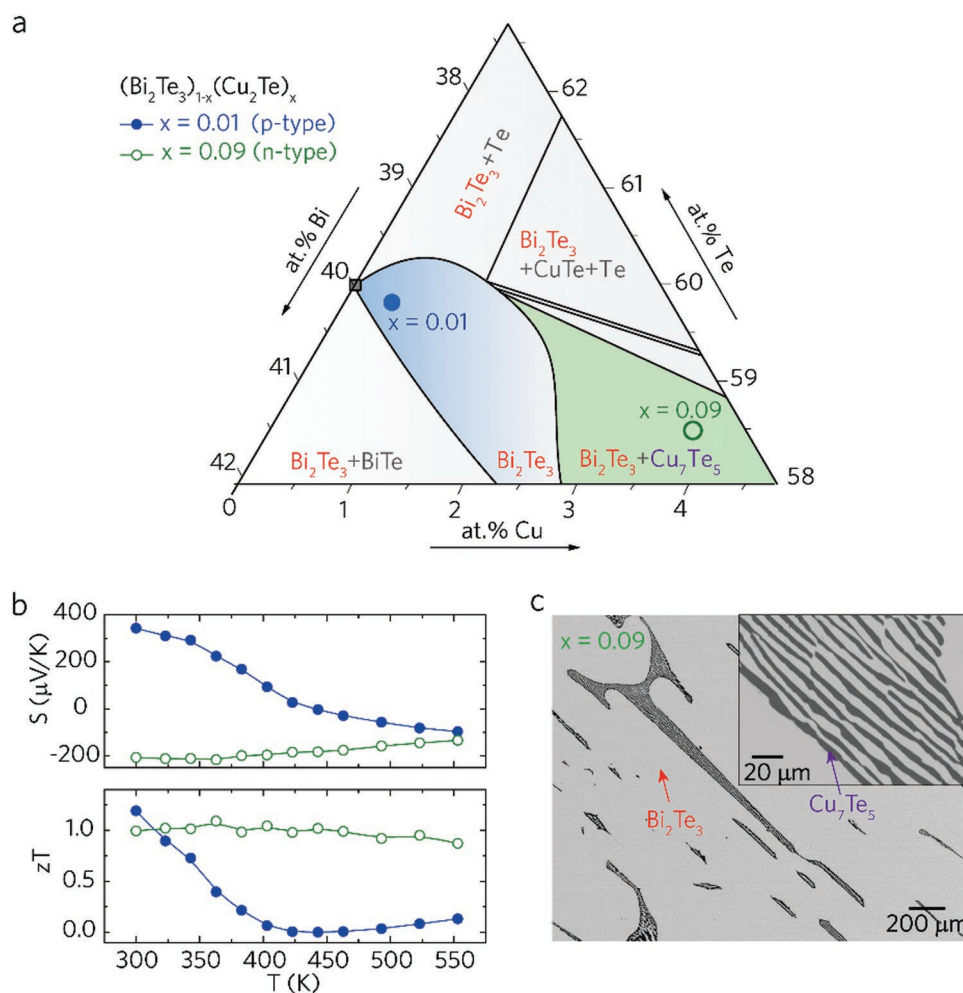


**Figure 4.** a) Enlarged isothermal section of Bi–Te–Cu, superimposed with the nominal compositions of two alloys:  $(\text{Bi}_2\text{Te}_3)_{0.99}(\text{Cu}_2\text{Te})_{0.01}$  ( $x = 0.01$ ) and  $(\text{Bi}_2\text{Te}_3)_{0.91}(\text{Cu}_2\text{Te})_{0.09}$  ( $x = 0.09$ ). b) Seebeck curves (upper panel) and  $zT$  curves (lower panel) for  $x = 0.01$  and  $x = 0.09$  alloys. c) The microstructures  $x = 0.09$  (n-type) exhibits a great deal amount of lamellar  $\text{Cu}_7\text{Te}_5$  precipitate. Adapted with permission.<sup>[86]</sup> Copyright 2018, Elsevier.

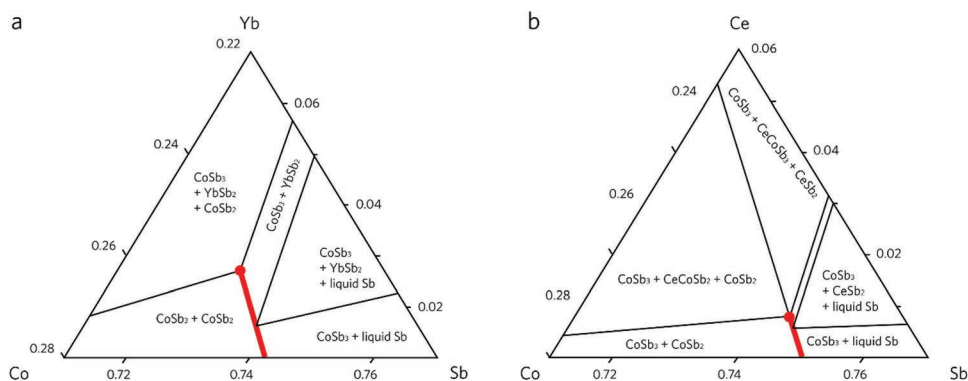


**Figure 5.** a,b) The isothermal section at 973 K near  $\text{CoSb}_3$  of the Yb–Co–Sb ternary system (31) (a) and the Ce–Co–Sb ternary system (b). The red line represents the  $\text{CoSb}_3$  single-phase solubility while the red point stands for the stable skutterudite composition with the maximum concentration of the filled element. a) Adapted with permission.<sup>[81]</sup> Copyright 2015, Elsevier. b) Adapted under the terms of the CC-BY Creative Commons Attribution 4.0 International License (<http://creativecommons.org/licenses/by/4.0/>).<sup>[82]</sup> Copyright 2015, Springer Nature.

Yb–Co–Sb and Ce–Co–Sb ternary systems have been experimentally determined. The red line represents the  $\text{CoSb}_3$  single-phase region, while the red point stands for the composition with the maximum concentration of filled element. For such filled skutterudites, their carrier concentration will increase with increasing filling atoms, which is crucial for improving the  $\sigma$  and PF. Acting as rattlers in phonon subsystem, increasing filler atoms reduces  $\kappa_L$ . Consequently, both p-type Yb– $\text{CoSb}_3$  ( $\text{Yb}_{0.3}\text{Co}_4\text{Sb}_{12}$ ) and n-type Ce– $\text{CoSb}_3$  ( $\text{Ce}_{0.17}\text{Co}_4\text{Sb}_{12}$ ) achieve a maximum  $zT$  value of 1.3 at 850 K as the concentration of filled elements reached the FFL.

Similarly, the origin of ultralow  $\kappa$  and high  $zT$  values in p-type Pb-doped  $\text{AgSbTe}_2$  and n-type Ge-doped  $\text{AgBiSe}_2$  have also been investigated with the assistance of phase diagram.<sup>[87,88]</sup> After adding the dopant,  $\delta\text{-Sb}_2\text{Te}$  and  $\text{Bi}_2\text{Se}_3$  nanoprecipitates will form in p-type Pb– $\text{AgSbTe}_2$  and n-type Ge– $\text{AgBiSe}_2$ , respectively. Due to the enhanced phonon scattering at nanoscale interfaces, the  $\kappa_L$  values of Pb– $\text{AgSbTe}_2$  and Ge– $\text{AgBiSe}_2$  are greatly reduced. In addition, the moiré fringes with a periodicity of 0.25 nm are found in the  $\text{Bi}_2\text{Se}_3$  nanoprecipitates, implying the existence of local mass fluctuation and superlattice structures as extra phonon scattering. It is imperative to employ phase-boundary mapping in well-known high- $zT$  TE materials such as  $\text{PbTe}$ ,<sup>[75,76]</sup>  $\text{SnSe}$ , and agrodites.<sup>[89,90]</sup>

#### 4. Liquid-Like Thermoelectrics

Materials with large atomic mass, weak interatomic bonding, complex crystal structure, strong anharmonicity, glassy structure, and low-lying optical vibrational modes are known to have low intrinsic  $\kappa_L$ . The  $\kappa_L$  can be further reduced through implementing point defects, dislocations, interfaces, and nanoprecipitates. In contrast, the intrinsically ultralow  $\kappa_L$  of mixed electronic ionic conductors stems from a distinct mechanism. Mixed electronic ionic conductors have dual hybridity: structural and conductive. In terms of structure, they consist of a rigid sublattice of fixed atoms and another sublattice of highly diffusive ions (cf. **Figure 6**), which exhibit liquid-like mobility at sufficiently high temperatures.<sup>[47–52]</sup> In terms of conduction, the charge and entropy flow are carried by electrons (holes) and

mobile ions. Even near room temperature, the diffusivities of  $\text{Cu}^+$  or  $\text{Zn}^{2+}$  ions in  $\beta\text{-Cu}_2\text{S}$ ,  $\beta\text{-Cu}_2\text{Se}$ ,  $\gamma\text{-Cu}_2\text{Te}$ , and  $\beta\text{-Zn}_4\text{Sb}_3$  are on the order of  $10^{-5}$ – $10^{-6}$   $\text{cm}^2 \text{s}^{-1}$ ,<sup>[91–94]</sup> while the diffusivity of  $\text{Ag}^+$  in  $\text{AgCrSe}_2$ ,  $\beta\text{-Ag}_2\text{Se}$ , and  $\alpha\text{-Ag}_2\text{Te}$  is on the order of  $10^{-1}$ – $10^{-3}$   $\text{cm}^2 \text{s}^{-1}$ .<sup>[48,95,96]</sup> With such high diffusion rates, ions can jump from one equilibrium position to another in very short time and behave like a liquid. To describe the electrical and thermal properties of such “liquid-like” TE materials, Chen and co-workers have proposed the concept of “phonon-liquid electron-crystal.” (PLEC).<sup>[47]</sup>

In a crystalline solid,  $\kappa_L$  can be expressed by  $\kappa_L = 1/3(C_V v l)$ ,<sup>[97]</sup> in which  $C_V$  is the isochoric heat capacity,  $v$  is the sound velocity, and  $l$  is the phonon MFP. Thermodynamically,  $C_V$  will approach the Dulong–Petit limit ( $3N_A R$ ), where  $N_A$  is the number of atoms per unit volume and  $R$  is the ideal gas constant. The experimentally measured heat capacity is the isobaric heat capacity  $C_P$ , rather than  $C_V$ . The presence of anharmonicity and the resulting thermal expansion ensures  $C_P \geq C_V$ ; if  $C_P$  is lower than the Dulong–Petit limit, even more so is  $C_V$ . As known, liquid cannot sustain transverse (shear) modes; hence, the partial loss of transverse modes in liquid-like materials leads to a lower-than-Dulong–Petit-limit  $C_V$  and provides a unique way of reducing  $\kappa_L$ .<sup>[47,98,99]</sup> It is worth noting that

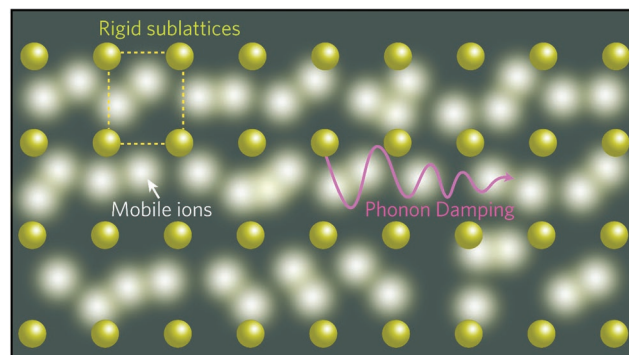


**Figure 6.** Schematic diagram of liquid-like TE materials. The arrows indicate the mobile ions that can travel within the rigid sublattices. The migrating ions are effective in damping the lattice vibrations, which reduces  $\kappa_L$ .

the longitudinal speed of sound ( $v_l$ ) in  $\text{Cu}_2\text{S}$  is much higher than that of  $\text{Cu}_2\text{Se}$ .<sup>[99]</sup> Nevertheless, the shear speed of sound ( $v_s$ ) in  $\text{Cu}_2\text{S}$  is remarkably lower than that of  $\text{Cu}_2\text{Se}$  due to the stronger ion migration. This explains that why  $\text{Cu}_2\text{S}$  has a relatively lower  $\kappa_l$  than that of  $\text{Cu}_2\text{Se}$ .<sup>[99,100]</sup>  $\beta\text{-Cu}_2\text{S}$ ,<sup>[99]</sup>  $\beta\text{-Cu}_2\text{Se}$ ,<sup>[47]</sup> and  $\text{AgCrSe}_2$ <sup>[98]</sup> demonstrate a  $C_p$  lower than the Dulong–Petit limit at high temperatures, while  $\gamma\text{-Cu}_2\text{Te}$ ,<sup>[101]</sup>  $\beta\text{-Ag}_2\text{Se}$ ,<sup>[102]</sup>  $\alpha\text{-Ag}_2\text{Te}$ ,<sup>[103,104]</sup> and  $\beta\text{-Zn}_4\text{Sb}_3$ <sup>[105]</sup> have a  $C_p$  slightly higher than the Dulong–Petit limit. Moreover, the migrating ions will create static and dynamic disorder that can inhibit the propagation of phonon modes and dampen phonon modes.

With the presence of secondary nanoprecipitate, the phonon MFP of liquid-like TE material can be further shortened. For example, the phonon MFP of  $\text{Cu}_2\text{Se}$  grown from the melt is 1.5 Å at room temperature.<sup>[106]</sup> The value is much smaller than the MFPs of  $\text{Bi}_2\text{Te}_3$ ,  $\text{CoSb}_3$ , and  $\text{PbTe}$ ,<sup>[107–109]</sup> which are 1.8, 4.5, and 3.2 Å at room temperature, respectively. The phonon MFP can be further decreased to 1.15 Å in  $\text{Cu}_2\text{Se}$  samples prepared by nonequilibrium recipes due to enhanced phonon scattering at randomly oriented grain boundaries.<sup>[110]</sup> While phonon modes in the entire Brillouin zone contribute to heat capacity, only those with finite group velocities contribute to the lattice thermal conductivity; thus, the estimated phonon MFP is the lower limit of actual phonon MFP. When a small amount of  $\text{CuInSe}_2$  and carbon nanotubes is incorporated into the  $\text{Cu}_2\text{Se}$  matrix, the maximum  $zT$  achieved can reach as high as 2.5 at 850 K and 2.4 at 1000 K due to the significant reduction of  $\kappa$ .<sup>[111,112]</sup> Notably, the  $\kappa_l$  calculated according to the Lorentz constant of  $1.6 \times 10^8 \text{ W } \Omega \text{ K}^{-2}$  is negative, and the reason is still unclear. It is found that the highly diffusive ions and nonequilibrium grain boundaries weaken the phase stability, especially at high temperature in the presence of an electric field and temperature gradient (Table 1). This is a serious issue for commercial applications and must be solved.<sup>[113]</sup>

## 5. Summary and Outlook

The development of thermoelectric materials and devices has recently drawn much attention. Despite newly discovered materials and many recent advances, the selection rules of parent compounds, and the subsequent doping, alloying, and compositing routine have remained unchanged for a few decades. There is a pressing demand for conceptual and methodological breakthroughs toward next-generation thermoelectric materials. In this review article, it is not our intention to exhaust the recent advances of all important topics; rather, we focused on three emerging thermodynamic routes, aka, entropy engineering, phase-boundary mapping, and liquid-like thermoelectrics. These thermodynamic routes have demonstrated their efficacy in a wide range of thermoelectric materials and provided new perspectives, e.g., the interplay between short-range disorder and high-symmetry long-range order in high-entropy materials, the precise control of compositions, phase stability, and microstructures via phase-boundary mapping, and the dual hybridity in crystal structure and electrical conduction in liquid-like thermoelectric materials. These results, along with the light shed by novel organic–inorganic hybrids and new degrees of freedom in transport properties,<sup>[114,115]</sup> beckon to a

multidisciplinary community to develop next-generation thermoelectric materials.

## Acknowledgements

P.-C.W., C.-N.L., H.-J.W., D.Y., and J.H. contributed equally to this work. C.-N.L. and J.-W.Y. would like to acknowledge the financial support from the Ministry of Science and Technology, Taiwan through the grant MOST 107-2923-E-007-007-MY2 and the “High Entropy Materials Center” at National Tsing Hua University, Taiwan. H.-J.W. would like to acknowledge the financial support from the Young Scholar fellowship program by the Ministry of Science and Technology in Taiwan through the grant MOST 108-2636-E-110-001. D.W.Y. and X.F.T. would like to acknowledge the financial support from the Natural Science Foundation of China through Grant No. 51632006, 51521001, and 51872219. J.-H.H. would like to acknowledge the financial support from KAUST. S.L. acknowledges the National Natural Science Foundation of China (Grant No. 61728403) and Zhejiang Provincial Natural Science Foundation of China (Grant No. LZ18E030001).

## Conflict of Interest

The authors declare no conflict of interest.

## Keywords

high-entropy alloys, liquid-like thermoelectrics, phase-boundary mapping, thermodynamics, thermoelectrics

Received: October 2, 2019

Revised: November 15, 2019

Published online: February 12, 2020

- [1] G. J. Snyder, A. H. Snyder, *Energy Environ. Sci.* **2017**, *10*, 2280.
- [2] J. R. D. Retamal, C. F. Kang, D. H. Lien, W. C. Kuo, Z. Y. Juang, M. L. Tsai, C. H. Ho, J. Y. Juang, V. K. S. Hsiao, Y. H. Chu, J. L. Li, Y. Wu, J. H. He, *Adv. Mater.* **2018**, *30*, 1705385.
- [3] Y. Pan, Y. Qiu, I. Witting, L. G. Zhang, C. G. Fu, J. W. Li, Y. Huang, F. H. Sun, J. Q. He, G. J. Snyder, C. Felser, J. F. Li, *Energy Environ. Sci.* **2019**, *12*, 624.
- [4] T. J. Zhu, Y. T. Liu, C. G. Fu, J. P. Heremans, J. G. Snyder, X. B. Zhao, *Adv. Mater.* **2017**, *29*, 1605884.
- [5] C. Xiao, Z. Li, K. Li, P. C. Huang, Y. Xie, *Acc. Chem. Res.* **2014**, *47*, 1287.
- [6] A. M. Dehkordi, M. Zebarjadi, J. He, T. M. Tritt, *Mater. Sci. Eng., R* **2015**, *97*, 1.
- [7] Z. W. Chen, B. H. Ge, W. Li, S. Q. Lin, J. W. Shen, Y. J. Chang, R. Hanus, G. J. Snyder, Y. Z. Pei, *Nat. Commun.* **2017**, *8*, 13828.
- [8] K. Biswas, J. Q. He, Q. C. Zhang, G. Y. Wang, C. Uher, V. P. Dravid, M. G. Kanatzidis, *Nat. Commun.* **2011**, *3*, 160.
- [9] S. I. Kim, K. H. Lee, H. A. Mun, H. S. Kim, S. W. Hwang, J. W. Roh, D. J. Yang, W. H. Shin, X. S. Li, Y. H. Lee, G. J. Snyder, S. W. Kim, *Science* **2015**, *348*, 109.
- [10] J. F. Li, W. S. Liu, L. D. Zhao, M. Zhou, *NPG Asia Mater.* **2010**, *2*, 152.
- [11] G. S. Nolas, J. L. Cohn, G. A. Slack, *Phys. Rev. B* **1998**, *58*, 164.
- [12] K. Biswas, J. Q. He, I. D. Blum, C. I. Wu, T. P. Hogan, D. N. Seidman, V. P. Dravid, M. G. Kanatzidis, *Nature* **2012**, *489*, 414.



- [13] H. S. Kim, W. S. Liu, G. Chen, C. W. Chua, Z. F. Ren, *Proc. Natl. Acad. Sci. USA* **2015**, *112*, 8205.
- [14] G. J. Snyder, E. S. Toberer, *Nat. Mater.* **2008**, *7*, 105.
- [15] M. S. Dresselhaus, G. Chen, M. Y. Tang, R. G. Yang, H. Lee, D. Z. Wang, Z. F. Ren, J. P. Fleurial, P. Gogna, *Adv. Mater.* **2007**, *19*, 1043.
- [16] A. J. Minnich, M. S. Dresselhaus, Z. F. Ren, G. Chen, *Energy Environ. Sci.* **2009**, *2*, 466.
- [17] Y. Z. Pei, H. Wang, G. J. Snyder, *Adv. Mater.* **2012**, *24*, 6125.
- [18] Q. Zhang, Y. M. Sun, W. Xu, D. B. Zhu, *Adv. Mater.* **2014**, *26*, 6829.
- [19] J. W. Fergus, *J. Eur. Ceram. Soc.* **2012**, *32*, 525.
- [20] M. He, M. F. Qiu, Z. Q. Lin, *Energy Environ. Sci.* **2013**, *6*, 1352.
- [21] B. Russ, A. Gludell, J. J. Urban, M. L. Chabiny, R. A. Segalman, *Nat. Rev. Mater.* **2016**, *1*, 16050.
- [22] G. J. Tan, L. D. Zhao, M. G. Kanatzidis, *Chem. Rev.* **2016**, *116*, 12123.
- [23] J. H. Bahk, H. Y. Fang, K. Yazawa, A. Shakouri, *J. Mater. Chem. C* **2015**, *3*, 10362.
- [24] J. L. Blackburn, A. J. Ferguson, C. Cho, J. C. Grunlan, *Adv. Mater.* **2018**, *30*, 1704386.
- [25] X. Y. Zhou, Y. C. Yan, X. Lu, H. T. Zhu, X. D. Han, G. Chen, Z. F. Ren, *Mater. Today* **2018**, *21*, 974.
- [26] S. Ortega, M. Ibanez, Y. Liu, Y. Zhang, M. V. Kovalenko, D. Cadavid, A. Cabot, *Chem. Soc. Rev.* **2017**, *46*, 3510.
- [27] J. P. Heremans, R. J. Cava, N. Samarth, *Nat. Rev. Mater.* **2017**, *2*, 17049.
- [28] W. Liu, K. Yin, Q. J. Zhang, C. Uher, X. F. Tang, *Nat. Sci. Rev.* **2017**, *4*, 611.
- [29] F. G. Eich, M. D. Ventra, G. Vignale, *J. Phys.: Condens. Matter* **2017**, *29*, 063001.
- [30] J. W. Yeh, S. K. Chen, S. J. Lin, J. Y. Gan, T. S. Chin, T. T. Shun, C. H. Tsau, S. Y. Chang, *Adv. Energy Mater.* **2004**, *6*, 299.
- [31] O. N. Senkov, J. D. Miller, D. B. Miracle, C. Woodward, *Nat. Commun.* **2015**, *6*, 6529.
- [32] Y. Zhang, T. T. Zuo, Z. Tang, M. C. Gao, K. A. Dahmen, P. K. Liaw, Z. P. Lu, *Prog. Mater. Sci.* **2014**, *61*, 1.
- [33] G. Anand, R. Goodall, C. L. Freeman, *Scr. Mater.* **2016**, *124*, 90.
- [34] H. R. Ma, J. Li, G. Yang, Y. M. Yang, X. J. Mao, C. C. Li, F. X. Yin, *J. Appl. Phys.* **2018**, *23*, 235104.
- [35] W. Liu, X. J. Tan, K. Yin, H. J. Liu, X. F. Tang, J. Shi, Q. J. Zhang, C. Uher, *Phys. Rev. Lett.* **2012**, *108*, 166601.
- [36] Y. Gelbstein, *Acta Mater.* **2013**, *61*, 1499.
- [37] A. Karati, M. Nagini, S. Ghosh, R. Shabadi, K. G. Pradeep, R. C. Mallik, B. S. Murty, U. V. Varadaraju, *Sci. Rep.* **2019**, *9*, 5331.
- [38] S. Roychowdhury, T. Ghosh, R. Arora, U. V. Waghmare, K. Biswas, *Angew. Chem., Int. Ed.* **2018**, *57*, 15167.
- [39] Z. Fan, H. Wang, Y. Wu, X. J. Liu, Z. P. Lu, *Mater. Res. Lett.* **2016**, *5*, 187.
- [40] S. Shafeie, S. Guo, Q. Hu, H. Fahlquist, P. Erhart, A. Palmqvist, *J. Appl. Phys.* **2015**, *118*, 184905.
- [41] S. Ohno, U. Aydemir, M. Amsler, J. H. Pohls, S. Chanakian, A. Zevalkink, M. A. White, S. K. Bux, C. Wolverton, G. J. Snyder, *Adv. Funct. Mater.* **2017**, *27*, 1606361.
- [42] S. Ohno, K. Imasato, S. Anand, H. Tamaki, S. D. Kang, P. Gorai, H. K. Sato, E. S. Toberer, T. Kanno, G. J. Snyder, *Joule* **2018**, *2*, 141.
- [43] P. Gorai, B. R. Ortiz, E. S. Toberer, V. Stevanovic, *J. Mater. Chem. A* **2018**, *6*, 13806.
- [44] C. M. Crawford, B. R. Ortiz, P. Gorai, V. Stevanović, E. S. Toberer, *J. Mater. Chem. A* **2018**, *6*, 24175.
- [45] B. R. Ortiz, K. Gordiz, L. C. Gomes, T. Braden, J. M. Adamczyk, J. X. Qu, E. Ertekin, E. S. Toberer, *J. Mater. Chem. A* **2019**, *7*, 621.
- [46] Y. L. Tang, Y. T. Qiu, L. L. Xi, X. Shi, W. Q. Zhang, L. D. Chen, S. M. Tseng, S. W. Chen, G. J. Snyder, *Energy Environ. Sci.* **2014**, *7*, 812.
- [47] H. Liu, X. Shi, F. Xu, L. Zhang, W. Zhang, L. Chen, Q. Li, C. Uher, T. Day, G. J. Snyder, *Nat. Mater.* **2012**, *11*, 422.
- [48] K. Zhao, P. Qiu, Q. Song, A. B. Blichfeld, E. Eikeland, D. Ren, B. Ge, B. B. Iversen, X. Shi, L. Chen, *Mater. Today Phys.* **2017**, *1*, 14.
- [49] K. Zhao, A. B. Blichfeld, H. Chen, Q. Song, T. Zhang, C. Zhu, D. Ren, R. Hanus, P. Qiu, B. B. Iversen, F. Xu, G. J. Snyder, X. Shi, L. Chen, *Chem. Mater.* **2017**, *29*, 6367.
- [50] B. B. Jiang, P. F. Qiu, H. Y. Chen, Q. H. Zhang, K. P. Zhao, D. D. Ren, X. Shi, L. D. Chen, *Chem. Commun.* **2017**, *53*, 11658.
- [51] X. Shi, L. Chen, *Nat. Mater.* **2016**, *15*, 691.
- [52] W. Qiu, L. Xi, P. Wei, X. Ke, J. Yang, W. Zhang, *Proc. Natl. Acad. Sci. USA* **2014**, *111*, 15031.
- [53] C. Y. Cheng, Y. C. Yang, Y. Z. Zhong, Y. Y. Chen, T. Hsu, J. W. Yeh, *Curr. Opin. Solid State Mater. Sci.* **2017**, *21*, 299.
- [54] R. H. Liu, H. Y. Chen, K. P. Zhao, Y. T. Qin, B. B. Jiang, T. S. Zhang, G. Sha, X. Shi, C. Uher, W. Q. Zhang, L. D. Chen, *Adv. Mater.* **2017**, *29*, 1702712.
- [55] L. P. Hu, Y. Zhang, H. J. Wu, J. Q. Li, Y. Li, M. McKenna, J. He, F. S. Liu, S. J. Pennycook, X. R. Zeng, *Adv. Energy Mater.* **2018**, *8*, 1802116.
- [56] S. A. Yamini, H. Wang, Z. M. Gibbs, Y. Z. Pei, S. X. Dou, G. J. Snyder, *Phys. Chem. Chem. Phys.* **2014**, *16*, 1835.
- [57] G. J. Tan, F. Y. Shi, S. Q. Hao, H. Chi, L. D. Zhao, C. Uher, C. Wolverton, V. P. Dravid, M. G. Kanatzidis, *J. Am. Chem. Soc.* **2015**, *137*, 5100.
- [58] L. Wu, X. Li, S. Wang, T. Zhang, J. Yang, W. Zhang, L. Chen, J. Yang, *NPG Asia Mater.* **2017**, *9*, e343.
- [59] A. F. Ioffe, *Semiconductor Thermoelements and Thermoelectric Cooling*, Inforsearch Ltd. London, UK **1957**.
- [60] P. C. Wei, T. S. Huang, S. W. Lin, G. Y. Guo, Y. Y. Chen, *J. Appl. Phys.* **2015**, *118*, 165102.
- [61] D. L. Medlin, G. J. Snyder, *Curr. Opin. Colloid Interface Sci.* **2009**, *14*, 226.
- [62] B. Ruiz-Yi, J. K. Bunn, D. Stasak, A. Mehta, M. Besser, M. J. Kramer, I. Takeuchi, J. Hatrick-Simpers, *ACS Comb. Sci.* **2016**, *18*, 596.
- [63] F. Otto, Y. Yang, H. Bei, E. P. George, *Acta Mater.* **2013**, *61*, 2628.
- [64] K. Bergum, T. Ikeda, G. J. Snyder, *J. Solid State Chem.* **2011**, *184*, 2543.
- [65] P. F. P. Poudeu, J. D'Angelo, H. J. Kong, A. Downey, J. L. Short, R. Pcionek, T. P. Hogan, C. Uher, M. G. Kanatzidis, *J. Am. Chem. Soc.* **2006**, *128*, 14347.
- [66] C. Xiao, J. Xu, B. Cao, K. Li, M. Kong, Y. Xie, *J. Am. Chem. Soc.* **2012**, *134*, 7971.
- [67] Y. F. Liu, M. H. Zhou, J. He, *Scr. Mater.* **2016**, *111*, 39.
- [68] J. Q. He, J. R. Sootsman, S. N. Girard, J. C. Zheng, J. G. Wen, Y. M. Zhu, M. G. Kanatzidis, V. P. Dravid, *J. Am. Chem. Soc.* **2010**, *132*, 8669.
- [69] N. A. Heinz, S. Howell, H. Wang, T. Ikeda, G. J. Snyder, *Phys. Status Solidi* **2012**, *209*, 2565.
- [70] H. W. Jeon, H. P. Ha, D. B. Hyun, J. D. Shim, *J. Phys. Chem. Solids* **1991**, *52*, 579.
- [71] L. P. Bulat, I. A. Drabkin, V. V. Karatayev, V. B. Osvenskii, Y. N. Parkhomenko, M. G. Lavrentev, A. I. Sorokin, D. A. Pshenai-Severin, V. D. Blank, G. I. Pivovarov, V. T. Bublik, N. Y. Tabachkova, *J. Electron. Mater.* **2013**, *42*, 2110.
- [72] B. Srinivasan, A. Gellé, F. Gucci, C. Boussard-Pledel, B. Fontaine, R. Gautier, J. F. Halet, M. J. Reece, B. Bureau, *Inorg. Chem. Front.* **2019**, *6*, 63.
- [73] W. Xie, J. He, H. J. Kang, X. Tang, S. Zhu, M. Laver, S. Wang, J. R. D. Copley, C. M. Brown, Q. Zhang, T. M. Tritt, *Nano Lett.* **2010**, *10*, 3283.
- [74] B. S. Kim, K. H. Lee, H. A. Mun, H. S. Kim, S. W. Hwang, J. W. Roh, D. J. Yang, W. H. Shin, X. S. Li, Y. H. Lee, G. J. Snyder, S. W. Kim, *Science* **2015**, *348*, 109.

- [75] Y. Pei, N. A. Heinz, A. LaLonde, G. J. Snyder, *Energy Environ. Sci.* **2011**, *9*, 3640.
- [76] H. J. Wu, W. J. Foo, W. Gierlotka, S. W. Chen, G. J. Snyder, *Mater. Chem. Phys.* **2013**, *141*, 758.
- [77] P. C. Wei, C. C. Yang, J. L. Chen, R. Sankar, C. L. Chen, C. H. Hsu, C. C. Chang, C. L. Chen, C. L. Dong, F. C. Chou, K. H. Chen, M. K. Wu, Y. Y. Chen, *Appl. Phys. Lett.* **2015**, *107*, 123902.
- [78] J. Nylén, M. Andersson, S. Lidin, U. Häussermann, *J. Am. Chem. Soc.* **2004**, *126*, 16306.
- [79] P. C. Wei, C. X. Cai, C. R. Hsing, C. M. Wei, S. H. Yu, H. J. Wu, C. L. Chen, D. H. Wei, D. L. Nguyen, M. M. C. Chou, Y. Y. Chen, *Sci. Rep.* **2019**, *9*, 8616.
- [80] J. Li, X. Zhang, S. Lin, Z. Chen, Y. Pei, *Chem. Mater.* **2017**, *29*, 605.
- [81] Y. Tang, S. W. Chen, G. J. Snyder, *J. Materiomics* **2015**, *1*, 75.
- [82] Y. Tang, R. Hanus, S. W. Chen, G. J. Snyder, *Nat. Commun.* **2015**, *6*, 7584.
- [83] D. G. Cahill, S. K. Watson, R. O. Pohl, *Phys. Rev. B* **1992**, *46*, 6131.
- [84] E. Matsuoka, S. Narazu, K. Hayashi, K. Umeo, T. Takabatake, *J. Appl. Phys.* **2006**, *75*, 14602.
- [85] M. Paliwal, I. H. Jung, *CALPHAD: Comput. Coupling Phase Diagrams Thermochem.* **2009**, *33*, 744.
- [86] H. J. Wu, W. T. Yen, *Acta Mater.* **2018**, *157*, 33.
- [87] H. J. Wu, S. W. Chen, T. Ikeda, G. J. Snyder, *Acta Mater.* **2012**, *60*, 6144.
- [88] H. J. Wu, P. C. Wei, H. Y. Cheng, J. R. Deng, Y. Y. Chen, *Acta Mater.* **2017**, *141*, 217.
- [89] P. C. Wei, S. Bhattacharya, Y. F. Liu, F. Liu, J. He, Y. H. Tung, C. C. Yang, C. R. Hsing, D. L. Nguyen, C. M. Wei, M. Y. Chou, Y. C. Lai, T. L. Hung, S. Y. Guan, C. S. Chang, H. J. Wu, C. H. Lee, W. H. Li, R. P. Hermann, Y. Y. Chen, A. M. Rao, *ACS Omega* **2019**, *4*, 5442.
- [90] W. Li, S. Q. Lin, B. H. Ge, J. Yang, W. Q. Zhang, Y. Z. Pei, *Adv. Sci.* **2016**, *3*, 1600196.
- [91] M. K. Balapanov, I. G. Gafurov, U. K. Mukhamed'yanov, R. A. Yakshibaev, R. K. Ishembetov, *Phys. Status Solidi* **2004**, *241*, 114.
- [92] S. A. Danilkin, M. Avdeev, T. Sakuma, R. Macquart, C. D. Ling, M. Rusina, Z. Izaola, *Ionics* **2011**, *17*, 75.
- [93] R. A. Yakshibaev, N. N. Mukhamadeeva, R. F. Kadrgulov, *Phys. Status Solidi* **1990**, *121*, 111.
- [94] E. Chalfin, H. Lu, R. Dieckmann, *Solid State Ionics* **2007**, *178*, 447.
- [95] B. A. Boukamp, G. A. Wiegers, *Solid State Ionics* **1983**, *9–10*, 1193.
- [96] I. Rom, W. Sitte, *Solid State Ionics* **1994**, *70–71*, 147.
- [97] C. Kittel, P. McEuen, *Introduction to Solid State Physics*, Vol. 8, Wiley, New York, NY **1996**.
- [98] F. Gascoin, A. Maignan, *Chem. Mater.* **2011**, *23*, 2510.
- [99] Y. He, T. Day, T. Zhang, H. Liu, X. Shi, L. Chen, G. J. Snyder, *Adv. Mater.* **2014**, *26*, 3974.
- [100] D. Yang, X. Su, Y. Yan, J. He, C. Uher, X. Tang, *APL Mater.* **2016**, *4*, 116110.
- [101] S. Ballikaya, H. Chi, J. R. Salvador, C. Uher, *J. Mater. Chem. A* **2013**, *1*, 12478.
- [102] D. Yang, X. Su, F. Meng, S. Wang, Y. Yan, J. Yang, J. He, Q. Zhang, C. Uher, M. G. Kanatzidis, X. Tang, *J. Mater. Chem. A* **2017**, *5*, 23243.
- [103] K. Honma, K. Iida, *J. Appl. Phys.* **1985**, *54*, 2218.
- [104] K. Honma, K. Iida, *J. Appl. Phys.* **1987**, *56*, 1828.
- [105] S. Wang, X. Tan, G. Tan, X. She, W. Liu, H. Li, H. Liub, X. Tang, *J. Mater. Chem.* **2012**, *22*, 13977.
- [106] P. Lu, H. Liu, X. Yuan, F. Xu, X. Shi, K. Zhao, W. Qiu, W. Zhang, L. Chen, *J. Mater. Chem. A* **2015**, *3*, 6901.
- [107] B. Y. Yavorsky, N. F. Hinsche, I. Mertig, P. Zahn, *Phys. Rev. B* **2011**, *84*, 165208.
- [108] T. Caillat, A. Borshchevsky, J. P. Fleurial, *J. Appl. Phys.* **1996**, *80*, 4442.
- [109] J. P. Heremans, V. Jovic, E. S. Toberer, A. Saramat, K. Kurosaki, A. Charoenphakdee, S. Yamanaka, G. J. Snyder, *Science* **2008**, *321*, 554.
- [110] X. Su, F. Fu, Y. Yan, G. Zheng, T. Liang, Q. Zhang, X. Cheng, D. Yang, H. Chi, X. Tang, Q. Zhang, C. Uher, *Nat. Commun.* **2014**, *5*, 4908.
- [111] A. A. Olvera, N. A. Moroz, P. Sahoo, P. Ren, T. P. Bailey, A. A. Page, C. Uher, P. F. P. Poudeu, *Energy Environ. Sci.* **2017**, *10*, 1668.
- [112] R. Nunna, P. Qiu, M. Yin, H. Chen, C. Lidong, *Energy Environ. Sci.* **2017**, *10*, 1928.
- [113] P. F. Qiu, T. Mao, Z. F. Huang, X. G. Xia, J. C. Liao, M. T. Agne, M. Gu, Q. H. Zhang, D. D. Ren, S. Q. Bai, X. Shi, G. J. Snyder, L. D. Chen, *Joule* **2019**, *3*, 1538.
- [114] H. Jin, J. Li, J. Iocozzia, X. Zeng, P. C. Wei, C. Yang, N. Li, Z. Liu, J. H. He, T. Zhu, J. Wang, Z. Lin, S. Wang, *Angew. Chem., Int. Ed.* **2019**, *131*, 2.
- [115] J. He, T. M. Tritt, *Science* **2017**, *357*, 9997.